ACS APPLIED MATERIALS & INTERFACES

Research Article

www.acsami.org

Culturing Fibroblasts in 3D Human Hair Keratin Hydrogels

Shuai Wang,[†,○] Zhenxing Wang,[‡,§,∥,○] Selin Ee Min Foo,[⊥] Nguan Soon Tan,[⊥,#] Yuan Yuan,[▽] Weisi Lin,[▽] Zhiyong Zhang,[*,‡,§,∥] and Kee Woei Ng[*,†]

[†]School of Materials Science and Engineering, Nanyang Technological University, N4.1, 50 Nanyang Avenue, Singapore 639798, Singapore

[‡]Department of Plastic and Reconstructive Surgery, Shanghai Ninth People's Hospital, School of Medicine, and [§]Shanghai Key Laboratory of Tissue Engineering, Shanghai Jiao Tong University, 639 Zhizaoju Road, Huangpu District, Shanghai, 200011, People's Republic of China

[∥]National Tissue Engineering Center of China, 68 Jiang Chuan East Road, Min Hang District, Shanghai, 200241, People's Republic of China

[⊥]School of Biological Sciences, Nanyang Technological University, 60 Nanyang Drive, Singapore 637551, Singapore

[#]Institute of Molecular and Cell Biology, A*STAR, 61 Biopolis Drive, Proteos, Singapore 138673, Singapore

[▽]School of Computer Engineering, Nanyang Technological University, N4, 50 Nanyang Avenue, Singapore 639798, Singapore

ABSTRACT: Human hair keratins are readily available, easy to extract, and eco-friendly materials with natural bioactivities. Keratin-based materials have been studied for applications such as cell culture substrates, internal hemostats for liver injury, and conduits for peripheral nerve repair. However, there are limited reports of using keratin-based 3D scaffolds for cell culture in vitro. Here, we describe the development of a 3D hair keratin hydrogel, which allows for living cell encapsulation under near physiological conditions. The convenience of making the hydrogels from keratin solutions in a simple and controllable manner is demonstrated, giving rise to constructs with tunable physical properties. This keratin hydrogel is comparable to collagen hydrogels in supporting the viability and proliferation of L929 murine fibroblasts. Notably, the keratin hydrogels contract less significantly as compared to the collagen hydrogels, over a 16-day culture period. In addition, preliminary in vivo studies in immunocompetent animals show mild acute host tissue response. These results collectively demonstrate the potential of cell-loaded keratin hydrogels as 3D cell culture systems, which may be developed for clinically relevant applications.

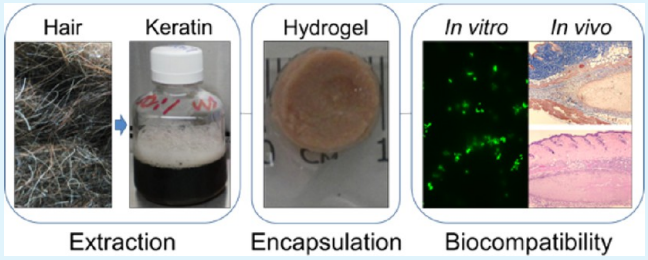

KEYWORDS: *keratin, hydrogel, 3D cell culture, fibroblast, cell compliance, tissue engineering*

1. INTRODUCTION

Conventional 2D cell culture systems are oversimplified models as compared to natural tissues. In those models, cells are grown on flat surfaces where tissue-specific cell arrangement, cell−matrix interactions, and cell−cell interactions are either lost or highly biased.[1] 3D cell culture systems have therefore become popular for a variety of purposes including drug screening, disease modeling, cell biology research, and tissue engineering.[2−4] Consequently, a number of 3D cell culture systems have been developed using synthetic or natural materials. Among those, protein-based materials (collagen, gelatin, silk, elastin, etc.) have proven advantageous as they are made up of amino acids, which are similarly found in natural tissues. Therefore, they can be degraded by enzymatic or hydrolytic processes and be cleared through the hosts' native physiological processes.[5,6] In addition, some of them inherit sequences with unique bioactivities, for example, cell binding motifs that support cell attachment and proliferation.[7−9] However, producing protein-based scaffolds on a large scale for clinical applications has been hindered by the limited availability of these proteins. Current protein production technologies are lagging behind the demands of protein-based scaffold production. Between the two most established protein production methods, organic chemistry peptide synthesis is not able to produce functional proteins larger than 50 amino acids effectively, while recombinant protein technology is still not cost-effective at an industrial scale.[10,11] On the other hand, proteins extracted from various animals have raised issues such as immune intolerance and risks of cross-species disease transmissions.[12]

Human hair keratins have emerged as potential materials to address some of these challenges. They are readily available, of human origin, have the potential to be autologous, easy to extract, renewable, and possess relevant biochemical properties.[13,14] Although there are currently limited human keratin-

Received: November 5, 2014
Accepted: February 17, 2015
Published: February 17, 2015

DOI: 10.1021/acsami.5b00854
ACS Appl. Mater. Interfaces 2015, 7, 5187−5198

based products for clinical use, a considerable amount of work has already been done to demonstrate this material's versatility. Coatings, films, sponges, fibers, and gels have all been produced from human hair keratins.[13,15−17] Functional studies on various potential applications of these matrixes have also been reported. For example, replacing human amniotic membrane with keratin films for ocular surface reconstruction improved light transmission, enhanced mechanical strength, and gave comparable corneal epithelial cell growth.[18] Porous keratin sponges obtained by compression-molding followed by particulate-leaching[19] or lyophilization[20] can support high density cell culture over long-term,[20] and can be used for delivery of drugs or bioactive molecules.[21,22] Keratin can also be incorporated into hybrid matrixes. In keratin−gellan−chitosan ternary complexes, keratins formed particles on the fiber surfaces and resulted in improved mechanical strength and biodegradability.[23] Electrospinning of keratin−silk or keratin−poly(ethylene oxide) mixture can produce ultrafine fibers, which were cell compliant.[24,25] Keratin hydrogels can also be produced relatively easily because of the propensity of keratins to self-assemble into networks.[26] These have been used as hemostats for liver injury and neuron conducting materials for nerve repair.[27−29] However, despite ample reports on cell and tissue compliance of keratin-based 3D matrixes, systematic in vitro cell culture studies are limited. Developing a keratin-based 3D cell culture system would enable the investigation of cell−keratin matrix interactions under 3D conditions and also provide insights toward developing clinically relevant keratin-based templates for cell and drug delivery. We have previously demonstrated the feasibility of cell seeding onto keratin hydrogels, but cells localized predominantly on the gel surfaces.[30] Here, we describe the extension of our previous work, by developing an easy-to-perform method of encapsulating live cells in 3D keratin hydrogels under near physiological conditions, which allowed the maintenance of high cell viability over a 16-day culture period with minimal graft contraction.

2. EXPERIMENTAL DETAILS

2.1. Materials. Sodium sulfide (Na_2S), paraformaldehyde (PFA), citric acid, sodium citrate, proteinase K, Tris-saturated phenol (pH 7.9), sodium dodecyl sulfate (SDS), bovine serum albumin (BSA), 2,2-diphenyl-1-picrylhydrazyl (DPPH), L-cysteine, and dialysis tubing [molecular weight cut off (MWCO) = 12 400 Da] were purchased from Sigma-Aldrich. Rat tail collagen type I was purchased from BD biosciences. Dulbecco's modified Eagle's medium (DMEM), nonessential amino acids, L-glutamine, fetal bovine serum (BSA), sodium pyruvate, penicillin-streptomycin, and 0.25% trypsin were purchased from Gibco (Invitrogen). Sylgard 184 Silicone Elastomer kit was purchased from Dow Corning. PicoGreen DNA quantification kit and Live/Dead cell assay were purchased from Molecular Probes (Invitrogen). 660 nm protein quantification kit was purchased from Thermo Fisher Scientific.

2.2. Extraction and Purification of Human Hair Keratins. Random human hair samples were obtained from local hair salons, without any distinction regarding age, gender, or ethnic group. Raw hair was washed with soap and rinsed extensively with water before decontamination in 70% ethanol for 6 h. Cleaned hair was air-dried and delipidized with a mixture of chloroform and methanol (2:1 v/v) for 24 h. The hair was subsequently air-dried and cut into short fragments of about 1 cm in length. 50 g of hair fragments was immersed in 1 L of extraction solution made of 0.125 M sodium sulfide at pH 10−13.5. Sodium sulfide was used as a reducing agent to break the disulfide bonds in the hair fibers to solubilize keratin. The mixture was kept in an oven at 40 °C for 2 h. The resulting keratin extract mixture was filtered using filter paper, and the filtrate was exhaustively dialyzed against deionized water, using cellulose dialysis tubing. The deionized water was changed every 2 h for four times and then every 12 h for four times. Keratin concentration was quantified using the 660 nm protein assay kit and sterile-filtered using 0.2 μm cellulose filters. Typical yields using this method were between 20% and 30% based on dry hair mass. We had previously optimized our keratin extraction protocol as well as carried out extensive characterization (FTIR, SDS-PAGE, and Western blotting) of the extracted keratins to show that the extraction conditions did not degrade the keratin protein.[17,24,30]

2.3. Light Microscopy Imaging of Keratin Flocs. Keratin flocculation was triggered by mixing 1 mL of keratin solutions over a concentration range (0.2−4 mg/mL) with 1 mL of PBS/citrate buffer at pH 3.5, made from mixing 1 mL of PBS buffer with 0.1 mL of 0.1 M citrate buffer, to achieve solutions of final concentrations of 0.1−2 mg/mL. One drop of each of the flocculated keratin solution was immediately placed on glass slides and covered with a coverslip before imaging using an upright phase contrast light microscope (CKX41, Olympus, Japan).

2.4. UV−Vis Spectrometry. A UV−vis spectrophotometer (UV-1700, Shimadzu, Japan) was used to measure the absorbance profiles at the wavelength of 400 nm. Samples were measured using a quartz sample cell with a light path of 10 mm. The measured sample values were corrected with the sample buffers as background references. For measuring keratin solution turbidity at different pH, PBS/citrate buffers were prepared by mixing PBS with 0.1 M, pH 3 citrate buffer at the volume ratios of 10:0, 10:0.3, 10:0.5, 10:1, and 10:2. The resulting buffer pH values were 7.2, 4.5, 4, 3.5, and 3.3, respectively. Subsequently, 3 mL of keratin solution with concentration of 15 mg/mL was mixed with 3 mL of each PBS/citrate buffer. Two milliliter aliquots of each keratin sample mixture were measured with the UV−vis spectrophotometer immediately. The remaining samples were poured into 25 mm Petri dishes for digital imaging.

In the temperature-dependent gelation experiment, flocculated keratin samples were prepared by mixing 30 mL of keratin solution (15 mg/mL) with 30 mL of PBS/citrate buffer (pH 3.5 prepared as mentioned above). Two milliliter aliquots of the mixture were made for respective incubation treatment and times. Three incubation treatment groups were included: "PBS", "water", and "PBS, 4 °C". Each group was monitored over nine time points. For the "PBS" and "water" groups, incubation was carried out at 37 °C. At each time point, the flocculated keratin samples were centrifuged at 1000g for 10 min. After the supernatant was discarded, the remaining keratin floc pellets were resuspended in either 2 mL of PBS ("PBS" and "PBS, 4 °C" groups) or 2 mL of deionized water ("water" group). The resulting suspensions were measured immediately with the UV−vis spectrophotometer as described.

2.5. Differential Scanning Calorimetry (DSC). Prior to DSC measurements, the concentrations of soluble keratin and flocculated keratin samples were adjusted to 1 and 0.5 mg/mL, respectively. The experiments were carried out using 300 μL of each sample on a nanodifferential scanning calorimeter (nano-DSC, TA Instruments, U.S.) fitted with a capillary cell. Temperature was increased from room temperature to 125 °C at 1 °C/min, under a pressure of 3 atm.

2.6. Isothermal Titration Calorimetry (ITC). Keratin samples were analyzed using isothermal titration calorimetry (nano-ITC, TA Instruments, U.S.) at 25 °C. All samples were degassed prior to the experiment. For each run, 30 μL of 0.1 M citrate buffer at pH 3 was continuously injected into 300 μL of 1 mg/mL keratin solution in PBS, at the rate of 0.1 μL/s. Samples were rapidly mixed by vortexing at 350 rpm as measurements were recorded.

2.7. 2,2-Diphenyl-1-picrylhydrazyl (DPPH) Assay. DPPH working solution at 100 mM was prepared in buffered methanol prepared by mixing 40 mL of 0.1 M pH 5.5 acetate buffer with 60 mL of methanol. Samples of 100 μL were mixed with 100 μL of DPPH working solution. Reactions were carried out at room temperature for 30 min before absorbance measurements were recorded at 517 nm using a plate reader. A calibration curve was generated using a serial dilution of 50 mM L-cysteine.

2.8. Keratin Hydrogel Fabrication. Keratin solution was mixed with PBS/citrate buffer (pH 3.5, prepared as mentioned above) at the

DOI: 10.1021/acsami.5b00854
ACS Appl. Mater. Interfaces 2015, 7, 5187−5198

ratio of 1:1 v/v. The volume of keratin solution used was calculated according to the desired final keratin concentration, taking into consideration the required final scaffold volume as well as the starting keratin solution concentration. For example, to make a 15 mL keratin hydrogel scaffold with a final concentration of 25 mg/mL, 25 mL of keratin solution at 15 mg/mL was added to the premixed PBS/citrate buffer made up of 25 mL of PBS and 2.5 mL of citrate buffer (0.1 M, pH 3). The resulting mixture was gently inverted several times to initiate immediate flocculation. Flocculated keratin solution was kept in a 37 °C incubator for 12 h followed by centrifugation at 1000*g*. The clear supernatant was discarded, while the flocculated keratin pellet was mechanically dispersed and washed with PBS or basal DMEM. This washing step was repeated twice. Depending on the downstream application, after the last wash, flocculated keratin can be dispersed in PBS or cell culture medium. The final mixture volume was adjusted to 15 mL to achieve the final keratin concentration of 25 mg/mL. It was measured that 3% of the total protein remained in solution after flocculation and was lost in the supernatant upon centrifugation (data not shown).

2.9. Scanning Electron Microscopy (SEM). Keratin hydrogels made with different keratin concentrations were frozen at −80 °C for 48 h before freeze-drying. The resulting scaffolds were fractured with tweezers to expose clean cross sections. Samples were gold-sputtered at 18 mA for 10 s and observed with a scanning electron microscope (JSM-6360, JEOL, U.S.) at an accelerating voltage of 5 kV under high vacuum.

We characterized the pores within the hydrogel microarchitecture from the SEM images using image processing techniques. The pore areas were segmented on the basis of the brightness contrast against the surface of the material in local regions. We first divided the SEM images into small blocks with overlaps. Each image block then was converted to a binary image where the pore regions and material surface regions were separated. Finally, we fused all of the image blocks together to get a binary image with the same size of the original SEM image. An image filter was applied to this binary image to remove background noise. Statistical analyses of the pores were computed on the basis of the segmented binary image. This image processing program was written and run using MATLAB 8.3.

2.10. Oscillatory Rheology. The oscillatory rheology experiments were performed using a rheometer (Anton Paar, Germany) with a 25 mm diameter stainless steel parallel plate. Keratin hydrogels were cast in 25 mm Petri dishes with the concentrations of 15, 25, 40, and 50 mg/mL. The height of each sample was measured by lowering the parallel plate until it touched the sample surface without compressing it. For frequency sweep, the storage modulus (G') was monitored as a function of angular frequency. A preliminary strain sweep was carried out to determine the linear viscoelastic response range of the hydrogels to be below 5% strain before the frequency sweep analysis was done.

2.11. L929 Murine Fibroblast Encapsulation and Cultivation. L929 murine fibroblasts were routinely maintained in complete culture media (DMEM supplemented with 10% fetal bovine serum, 2 mM L-glutamine, 1 mM sodium pyruvate, 0.1 mM MEM nonessential amino acids, 100 units/mL penicillin, and 100 μg/mL streptomycin) at 37 °C and 5% CO_2. For encapsulation, cell suspensions were mixed with the prepared flocculated keratin/culture medium mixture at a density of 50 000 per mL (0.5 mL per 12 mm diameter customized mold). Mixing was done by careful and gentle pipetting to minimize cell damage. The cell suspensions were then loaded into respective containers (tissue culture plates or customized molds). Customized molds were prepared by adhering polyethylene rings of diameter 12 mm onto circular glass coverslips of diameter 20 mm using PDMS (Sylgard 184 Silicone Elastomer kit, Dow Corning), as depicted in Figure 2B. The PDMS was cured in an oven at 70 °C for 2 h, and the molds were subsequently sterilized with UV irradiation before they were used. To minimize defects, the cell-seeded hydrogels were kept untouched for 8 h in an incubator at 37 °C and 5% CO_2. Subsequently, fresh complete culture medium was gently added on top of the keratin hydrogels until they were fully submerged. Cell culture medium was changed every 2 days. As control, 1 mg/mL rat tail collagen type I hydrogels were prepared according to the manufacturer's instruction. The required volumes of collagen solution were neutralized with 1 M NaOH in PBS and then mixed quickly with cell suspensions followed by gelation at 37 °C. Fresh cell culture medium was added 1 h later and changed every 2 days.

2.12. Cell Viability and Proliferation. Cell distribution and viability were visualized by Live/Dead staining, according to the manufacturer's instructions. Live cells fluoresced green, while dead cell nuclei fluoresced red. Cell proliferation was monitored by quantifying double-stranded DNA (dsDNA) over time, using the PicoGreen assay. Unlike in conventional 2D cell culture, cells encapsulated in the keratin/collagen hydrogels had to be released from the 3D environment for efficient cell lysis and harvesting of dsDNA.[31] This process was followed by DNA/protein separation to remove excess proteins for more accurate quantification. Here, we used proteinase K to digest the keratin/collagen hydrogels. Before digestion, medium was removed as much as possible. Each sample was then incubated with 1 mL of 10 mM Tris-HCl pH8 buffer containing 0.5% SDS and 0.3 μg of proteinase K. Incubation was carried out at 37 °C overnight under constant agitation. All hydrogels after 4 days' culture were digested completely within 12 h of enzyme treatment. Those cultured more than 4 days were continuously digested by replenishing 0.3 μg of proteinase K to the digestion solution every 12 h until no visible fragments were left.

Digested samples were further purified using phenol. First, digested samples were volume adjusted from around 2 to 5 mL using deionized water. 1 mL of each digested sample was then mixed with 1 mL of Tris-saturated phenol. The mixtures were inverted several times until emulsions were formed. These were then centrifuged at 20 000*g* for 3 min to create two clearly visible separate phases. Polar DNA molecules were collected in the top aqueous phase, while denatured protein molecules were separated to the bottom organic phase. Without disrupting the organic phase, the top aqueous phase was carefully transferred to a new tube. One milliliter of chloroform was added to the separated aqueous phase, followed by repeating the same phase separation procedure. The second phase separation cycle was included to remove possible traces of phenol in the aqueous phase, which could interfere with the PicoGreen assay. DNA quantification was performed using the PicoGreen assay according to the manufacturer's instructions. Briefly, 100 μL of working PicoGreen reagent was mixed with 20 μL of sample in 96 well plates. After 5 min of incubation, fluorescence was measured by a plate reader at excitation and emission wavelengths of 480 and 520 nm, respectively. The amount of dsDNA in each sample was calculated from a calibration curve generated using dsDNA standards.

2.13. Histological Analysis. Cell-populated keratin hydrogels were fixed in 4% paraformaldehyde (PFA) in PBS for 48 h at room temperature, washed with PBS, and embedded in paraffin. Five micrometer thick cross sections were collected and stained with hematoxylin and eosin (H&E). Brightfield imaging was done on an upright light microscope (CKX41, Olympus, Japan).

2.14. Preliminary in Vivo Studies. All in vivo studies were carried out with ethical approvals from the institutional authorities. For short-term in vivo studies, female C57Bl/6 mice were anesthetized by isoflurane inhalation. Surgery sites were shaved before two 3 mm incisions were made on the dorsal skin of each mouse using surgical scissors. A subcutaneous pocket was made through the incision using a spatula. One keratin hydrogel disk (40 mg/mL, 3 mm in diameter and 2 mm thick) was inserted into each pocket. The incision was closed with adhesive skin closure tape. The mice were sacrificed at day 7 ($n = 2$), and the implants were retrieved and fixed with 4% paraformaldehyde. For long-term studies, Sprague−Dawley rats were used. Operational procedures were the same as described above, except that 1 mL of keratin hydrogel was injected into the subcutaneous compartments using a syringe through 30 mm incisions and closed with surgical sutures. Implants were retrieved after 90 days, as described above. All harvested samples were sectioned and processed for H&E and Masson's Trichrome staining using standard procedures.[32,33]

2.15. Statistical Analysis. All quantitative experiments were done in triplicate ($n = 3$) unless otherwise indicated. Relative values were expressed as percentages with respect to controls and compared using either 1-way ANOVA with Tukey's posthoc test or Student's t test. Differences with $p < 0.05$ were considered statistically significant.

DOI: 10.1021/acsami.5b00854
ACS Appl. Mater. Interfaces 2015, 7, 5187−5198

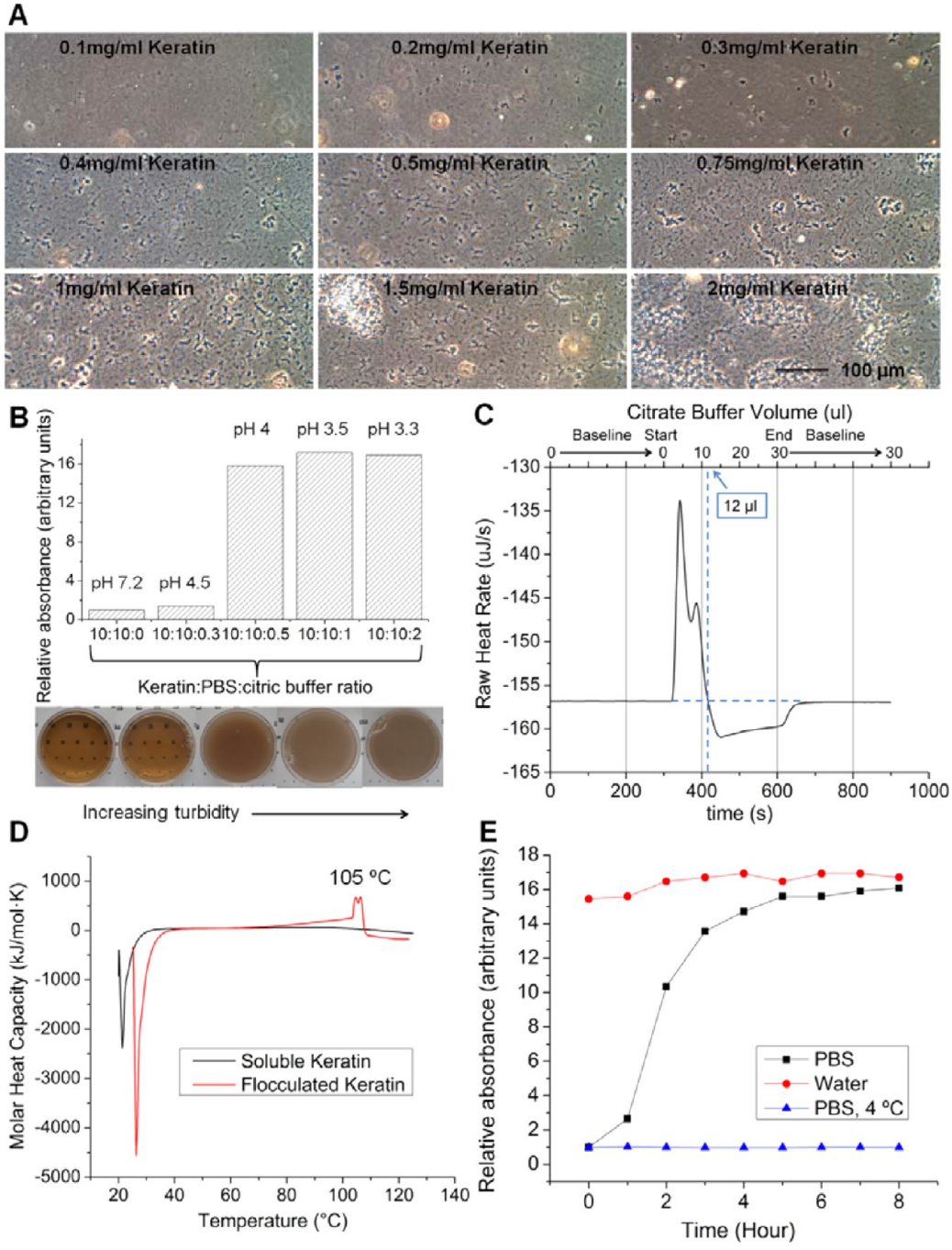

Figure 1. Establishing the three key factors in controlling keratin gelation: concentration, pH, and temperature. (A) Keratin samples of final concentrations ranging from 0.1 to 2 mg/mL at pH 3.5 were observed using phase contrast light microscopy. As keratin concentration increased, floc density and size also increased. Scale bar represents 100 μm. (B) Results from UV−vis spectrophotometry quantification of visible light absorbance over a decreasing pH range correlated with a corresponding increase in sample turbidity as a result of increased light scattering due to keratin flocculation. (C) Nano-ITC analysis revealed an endothermic keratin unfolding process that transited into an exothermic keratin flocculation process when a critical volume of 12 μL of citrate buffer was injected into 300 μL of keratin solution during the time period from 300 to 600 s. (D) Nano-DSC results of soluble keratin (black) and flocculated keratin (red) showed the appearance of an endothermic peak in flocculated keratin samples at around 105 °C, likely the result of heat-induced unfolding. (E) Stability of the keratin flocs and subsequent gelation was further correlated to temperature and incubation time by measuring visible light absorbance. Stability at neutral pH (PBS) was established after 5 h incubation at 37 °C.

3. RESULTS

3.1. Factors To Control Keratin Gelation: Concentration, pH, and Temperature. It is critical to control the keratin gelation process to optimize live cell encapsulation. Here, we identified three controllable factors: concentration, pH, and temperature. Keratin gelation process can be divided into two stages. The first stage involved the formation of keratin flocs. Many proteins have the tendency to undergo spontaneous association that is driven mainly by hydrophobic interactions. However, at neutral pH, keratin molecules carry net negative charges (pI < 7), which keep the molecules apart due to electrostatic repulsion. Thus, at neutral pH, keratin dissolves readily to give a brownish, semitransparent solution. By gradually

DOI: 10.1021/acsami.5b00854
ACS Appl. Mater. Interfaces 2015, 7, 5187−5198

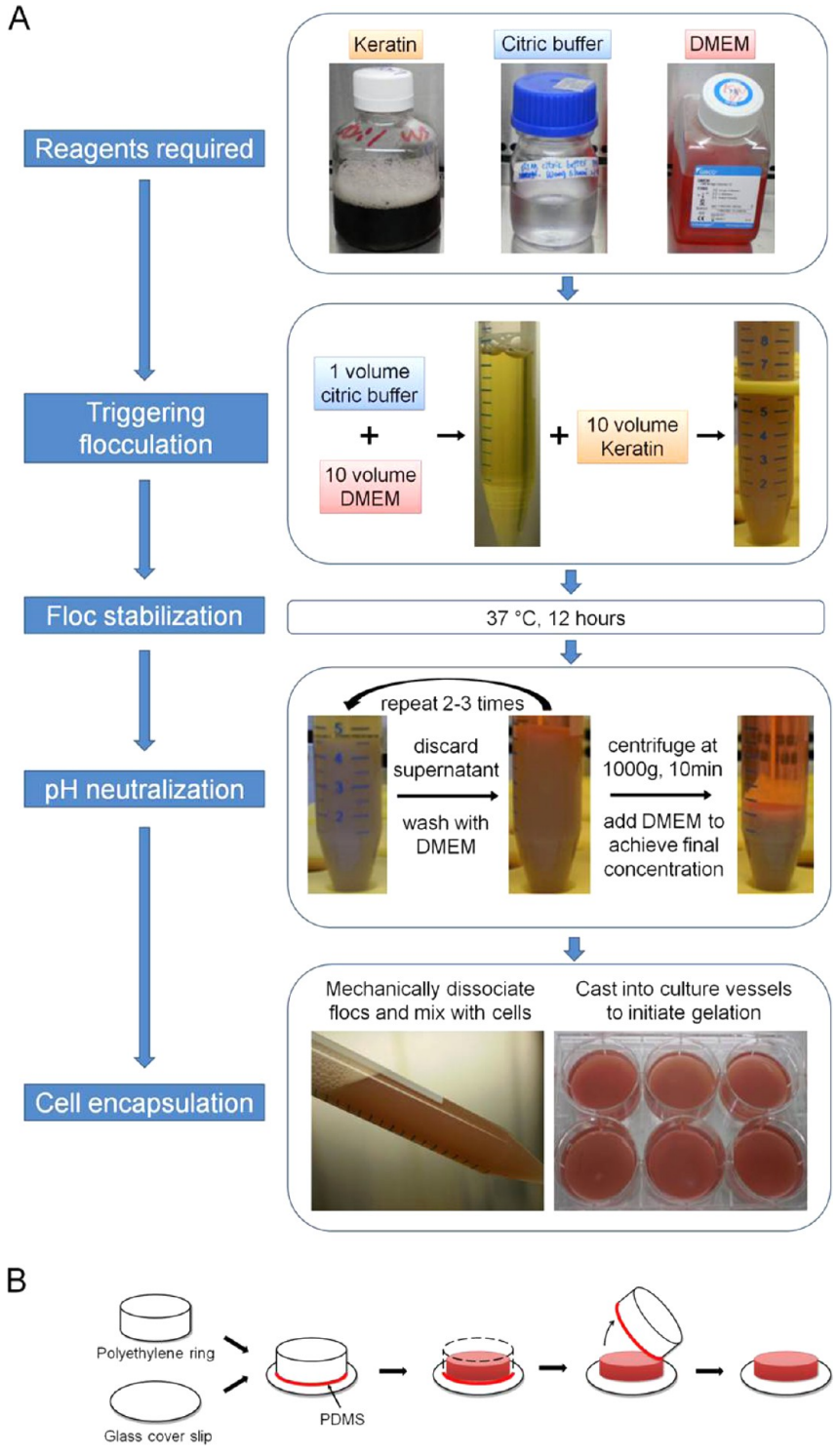

Figure 2. (A) Schematic illustration of the live cell encapsulation procedure in 3D keratin hydrogels. Keratin flocculation was first triggered at pH 3.5 by mixing the keratin solution with premixed PBS/citrate buffer. After 12 h incubation at 37 °C, stabilized keratin flocs were washed with neutral pH buffer (PBS or DMEM), followed by suspending living cells in cell culture medium and casting into culture vessels to allow for gelation. (B) Cell-seeded keratin hydrogels were also cast in custom-made molds assembled from polyethylene rings adhered onto glass coverslips using PDMS, as shown. These allowed convenient transportation of keratin hydrogels for downstream activities such as microscopy and histology processing.

lowering pH, the negative charges on keratin molecules are lost. Hydrophobic interactions became the dominant force, which results in keratin flocculation. This process was first noticed at pH 3.5 (Figure 1A). These resulting flocs appeared either as aggregates or as gel networks depending on keratin concentration. As keratin concentration increased from 0.1 to 2 mg/mL, the number of keratin flocs visibly increased as well. Clustering of keratin flocs began at higher concentrations such that by 2 mg/mL, the keratin flocs appeared to have self-assembled into interconnected networks.

We then explored the range of pH at which keratin flocculation was triggered, by visual inspection and quantifying visible light

DOI: 10.1021/acsami.5b00854
ACS Appl. Mater. Interfaces 2015, 7, 5187−5198

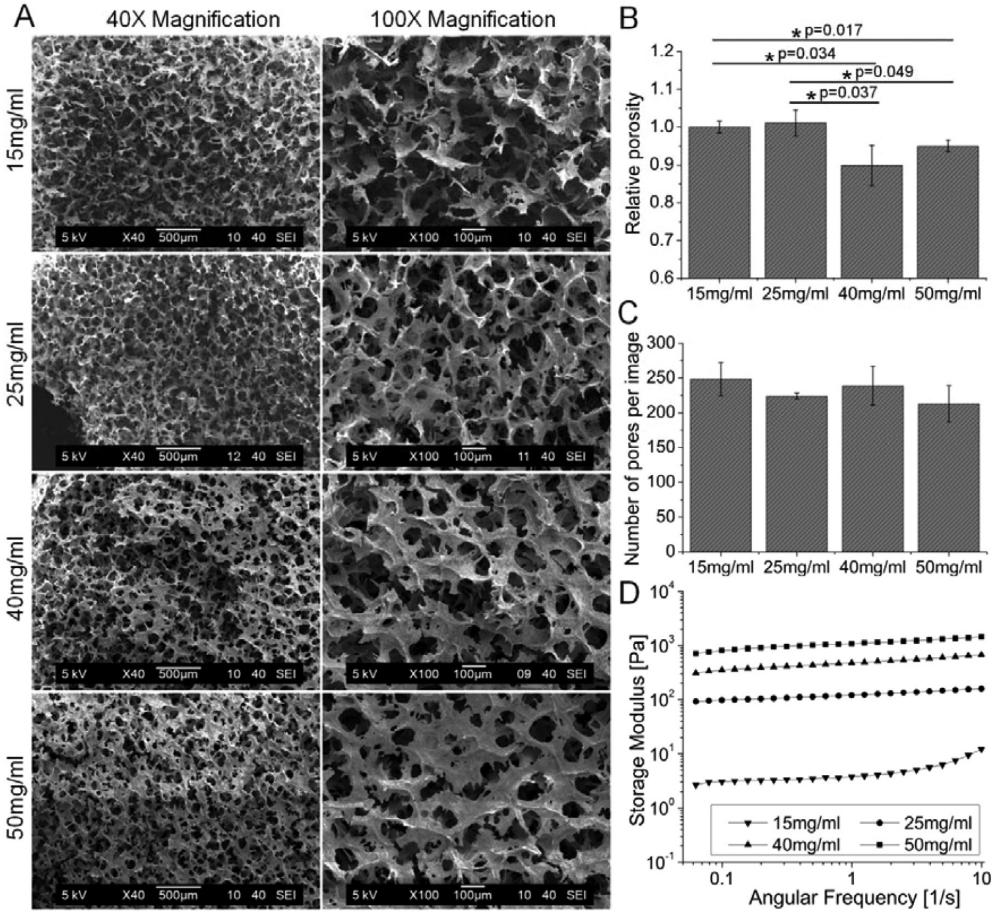

Figure 3. Physical and mechanical characterization of keratin hydrogels made from solutions of different keratin concentrations. (A) SEM images of freeze-dried hydrogels displayed porous microarchitectures of high pore interconnectivity and homogeneous pore structures. (B) Relative porosity change (n = 3) and (C) number of pores in relation to increasing keratin concentration (n = 3). (D) Plots of storage modulus, G', as a function of frequency suggest increased stiffness with higher keratin concentration.

absorbance (Figure 1B). At neutral pH, the keratin solution was brownish and semitransparent. By gradually lowering pH, flocculation occurred. As keratin flocs clustered and formed networks, they began to scatter light and result in the observed increase in turbidity. Consequently, the semitransparent keratin solutions became opaque gels. By measuring the absorbance of keratin solutions in the pH range of 3.3−7.2, we confirmed that keratin flocculation was triggered between pH 4 and 4.5, where the isoelectric point of the material lies.

To complement the turbidity measurements and microscopic observations, ITC was performed to find out the critical citrate buffer ratio at which keratin flocculation was triggered. Heat flow was monitored as citrate buffer was continuously injected into the keratin solution chamber. Similar to other proteins, keratin unfolded as pH was lowered, giving rise to the two endothermic peaks as shown in Figure 1C, suggesting a two-stage unfolding process. As unfolding continued and isoelectric point of the material was reached, hydrophobic regions became exposed and the net charge of the molecules became zero. Hydrophobic interaction became dominant and flocculation started. Unlike the endothermic unfolding process, the flocculation process was exothermic, which explained the appearance of a broad exothermic peak after 12 μL of citrate buffer was injected, indicating the onset of keratin flocculation. At this point, the keratin/PBS/citrate buffer ratio was 10:10:0.8, which was close to the ratio (10:10:0.3 to 10:10:0.5) predicted on the basis of turbidity measurements (Figure 1B). The delayed appearance of the exothermic peak was due to the overlap with the endothermic peaks resulting from protein unfolding.

Because of the pH-induced conformational changes, flocculated keratin became less resistant to heat, based on DSC analysis (Figure 1D). Native keratins are very stable, with melting points documented to be as high as 150−200 °C. As shown in Figure 1D, soluble keratins were found to be stable during the heating process. In comparison, flocculated keratin molecules, which were partially unfolded during the flocculation process, were less resistant to heat. An endothermic peak at around 105 °C was recorded, likely the result of heat-induced unfolding.

It was thus demonstrated that keratin flocculation was brought by conformational changes and charge neutralization as pH was lowered, which allowed hydrophobic interactions to dominate and bring about flocculation.

In the next step, we studied the stabilization of the keratin flocs, which required at least 5 h incubation at 37 °C, pH 3.5. Without this stabilizing process, keratin flocculation was easily reversed. As shown in Figure 1E, at time 0 after triggering the flocculation process (no stabilizing time) in the "PBS" group, resuspending the keratin flocs in PBS resulted in complete resolubilization. As a result, absorbance reading was recorded at a low background level. As the incubation time increased from 1 to 4 h, keratin flocs became increasingly stable, as seen from a significant increase in the absorbance readings. After at least 5 h

DOI: 10.1021/acsami.5b00854
ACS Appl. Mater. Interfaces 2015, 7, 5187−5198

incubation at 37 °C, resolubilization of the keratin was no longer possible, as seen from the absorbance readings reaching a plateau. On the other hand, resuspending keratin in the "water" group did not cause any resolubilization even without incubation time. This was because water has poor pH neutralizing capacity, and thus the resulting suspensions remained acidic.

We further found that this stabilizing process was temperature dependent. In the group suspended in PBS kept at 4 °C, keratin flocs always resolubilized regardless of incubation time, even though pH was neutral. In addition, stabilization of the keratin flocs was also achieved at a higher incubation temperature of 25 °C by doubling incubation time (data not shown). After stabilization, keratin flocs were washed with PBS or cell culture medium to neutralize pH to establish a physiological environment for live cell encapsulation. Formation of a 3D hydrogel occurred when the neutralized keratin flocs were left undisturbed for several hours. We speculate that formation of disulfide bonds between the free thiol groups of the cysteine residues in keratin played an important role in cross-linking the keratin flocs together. Using the DPPH assay, the free thiol group concentration in 25 mg/mL keratin solution was estimated to be 198 ± 30 μM (n = 4). On the basis of the key factors we have identified, we formulated a protocol for the encapsulation and cultivation of live cells in keratin hydrogels (Figure 2A). To facilitate handling of the hydrogels, we custom-made cylindrical molds using polyethylene rings adhered to glass coverslips with PDMS (Figure 2B).

3.2. Physical and Mechanical Properties of Keratin Hydrogels. The microarchitecture of the keratin hydrogels was characterized by SEM. Lyophilized keratin hydrogels had highly porous microarchitecture with interconnected pores (Figure 3A). At the concentration of 15 mg/mL, keratin hydrogels showed an interconnected network formed by branched leaflets. Increasing keratin concentration to 50 mg/mL reduced porosity (Figure 3B) but not number of pores (Figure 3C). Qualitatively, the size of major pores ranged from 50 to 200 μm and appeared to reduce with increasing keratin concentration.

The mechanical property of the keratin hydrogels was compared by measuring storage modulus using a rheometer (Figure 3B). Our results showed that by adjusting keratin final concentration from 15 to 50 mg/mL, keratin hydrogels could have their storage moduli increased by more than 200-fold (approximately 3 to 800 Pa). The higher end of this range corresponds to the storage moduli of natural soft tissues such as the brain.[34]

3.3. Encapsulation of L929 Fibroblasts in 3D Keratin Hydrogels. At day 2, randomly distributed single cells were observed in both collagen (1 mg/mL) and keratin (25 mg/mL) samples (Figure 4). At day 4, cell doublets were observed, indicating cell proliferation. At day 6, cell clusters were observed in both groups. At day 8, cell clusters increased in size as the result of sustained proliferation. Throughout 8 days of culture, dead cells were rarely found, which suggested L929 fibroblast viability was preserved during the encapsulation process and was maintained throughout the culture period.

L929 proliferation in keratin or collagen hydrogels was monitored by measuring the double-stranded DNA amount (dsDNA) over 16 days. In both materials, typical cell proliferation profiles were exhibited where after the initial lag phase, cells began to proliferate exponentially from day 4 on (1-way ANOVA; $p = 3.83 \times 10^{-05}$) and transited into a linear growth phase before reaching a plateau at day 12. At day 1, almost equal amounts of DNA were obtained for both keratin and collagen

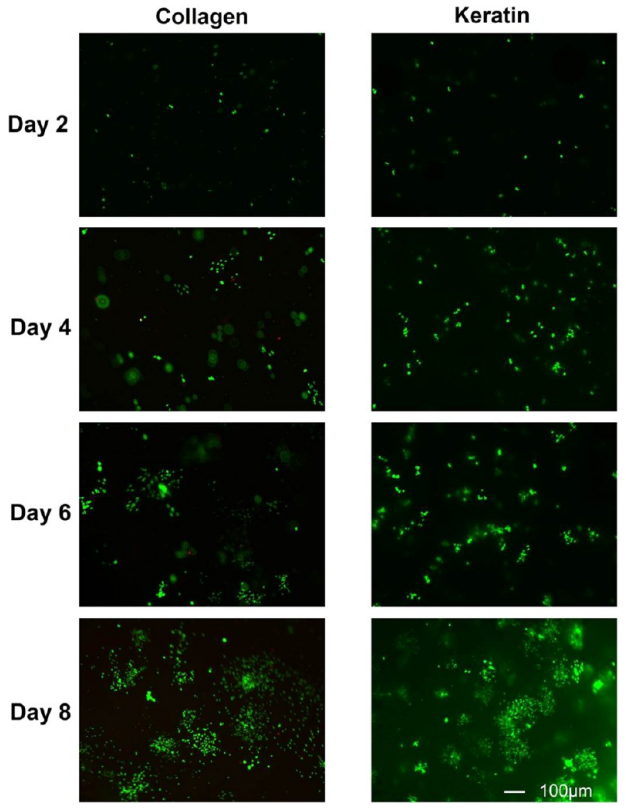

Figure 4. Fluorescence images of Live/Dead-stained L929 murine fibroblasts seeded in collagen or keratin hydrogels at 50 000 cells per mL. Cell doublets were observed from day 4. Growing cell clusters were observed at day 6 and most significantly at day 8, indicating rapid cell proliferation. Few dead cells were observed over the culture period. Scale bar is representative for all panels.

groups (Figure 5A). From day 2 to day 10, keratin groups led slightly in cell numbers. However, collagen groups caught up after day 10. Keratin groups reached maximum dsDNA content at day 12, while collagen groups reached their maximum at day 14. At day 16, both groups dropped in cell numbers. At the last stage (days 14 and 16), space limitations and nutrient transport efficiency probably became the more crucial limiting factors than other properties. In general, keratin hydrogels were as good as collagen hydrogels in terms of promoting L929 proliferation. Moreover, we observed interestingly that keratin hydrogels contracted significantly lesser than collagen hydrogels while having similar cell numbers. As shown in Figure 5B, collagen hydrogels contracted to approximately 6 mm in diameter at day 10, which was one-half of its initial size, while keratin hydrogels contracted only slightly by 2 mm in diameter. Both groups achieved maximum contraction at around day 8, and remained relatively unchanged until the cultures were terminated at day 16.

As fluorescence microscopy can only capture cells that were relatively near to the scaffold surface, we carried out histological analysis of the cross sections of the cell-loaded samples, stained with H&E, to evaluate cell distribution across the depth of the hydrogels (Figure 6). At days 2 and 6, most cells were found randomly distributed throughout the hydrogel, indicating good encapsulation efficiency. However, after 12 days of culture, more cells were observed on or near the hydrogel surfaces. That was likely because at the later stages of culture, cells migrated toward the surface or proliferated faster at the surface due to more efficient nutrient exchange. In addition, at day 12, cells were

DOI: 10.1021/acsami.5b00854
ACS Appl. Mater. Interfaces 2015, 7, 5187−5198

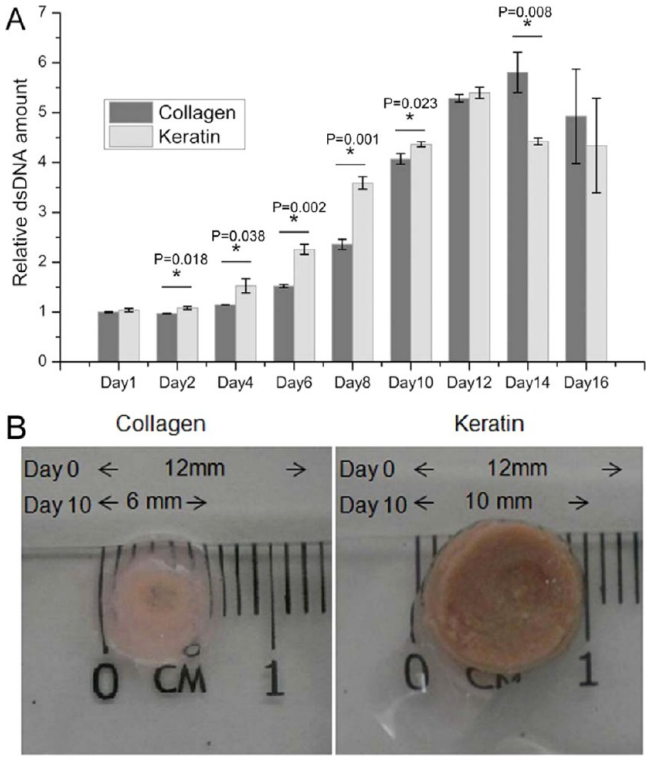

Figure 5. Cell proliferation and sample contraction. (A) Relative proliferation of L929 fibroblasts encapsulated in keratin hydrogels in comparison with collagen hydrogels. Data represent relative double-stranded DNA (dsDNA) amounts over 16 days of culture, normalized to collagen hydrogels at day 1, and presented as means ± standard deviation of triplicates. *Student's *t* test. (B) Comparison of cell-induced contraction in collagen and keratin hydrogels. Collagen hydrogels contracted by 6 mm (50%) while keratin hydrogels contracted by only 2 mm (17%) over the same culture period.

observed to express the typical spindle morphology of fibroblasts (Figure 6C1), suggesting adherence to the surrounding keratin matrix.

3.4. In Vivo Studies. The implanted keratin hydrogels remained intact after 7 days and were observed to be well integrated with the surrounding host tissue (Figure 7A,B). Fibrotic encapsulation around the hydrogels was mild. Significant cell infiltration into the keratin hydrogels was observed (Figure 7C,D). On the basis of cell morphology, both fibroblasts (spindle) and neutrophils (round with dense nuclei) were found surrounding the hydrogels as well as within. Some degree of matrix remodeling could be observed at the hydrogel–host tissue interface (Figure 7C,D). At day 90 postimplantation, about 30% of the keratin hydrogels remained detectable, based on volume. These were fragmented, avascular, and encapsulated by thin fibrotic capsules (Figure 7E,F).

4. DISCUSSION

Flocculation has been loosely defined as the process "in which particles in a colloid aggregate into larger clumps".[35] More specifically, it is the process of "contact and adhesion whereby dispersed molecules or particles are held together by weak physical interactions ultimately leading to phase separation by the formation of precipitates of larger than colloidal size."[36] On the basis of these definitions, we therefore refer to pH-induced formation of keratin aggregates from a solution of keratin molecules as a flocculation process. This results in loosely bonded aggregates that can be dissociated again by reversing pH, as shown by our results (Figure 1). In certain aspects, this mechanism of keratin gelation is similar to that of other natural protein gels (soy protein, egg protein, etc.) where various noncovalent linkages dominate, such as hydrophobic interactions, electrostatic interactions, hydrogen bonds, and van der Waals forces. Presumably, hydrophobic interactions play the most significant role in these protein systems.[37] On the basis of the fractal aggregation theory, the keratin molecules move freely in solution by Brownian motion, and form clusters when they collide with each other. These clusters then aggregate with other clusters to form the basic building blocks of the networks that eventually result in a hydrogel.[38] However, one distinct difference of hair keratins as compared to other protein systems is their high cysteine content. This allows the formation of disulfide bonds in oxidative conditions, which stabilize the keratin flocs by producing a cross-linked hydrogel (Figure 1). Therefore, by understanding and controlling the important factors affecting keratin flocculation, we not only have a mean to isolate, purify, and concentrate hair keratins, we can also use this knowledge to encapsulate living cells within keratin hydrogels.

Preformed matrixes in the forms of sponges and foams are alternative systems for 3D cell culture.[4,39] However, the difficulty of ensuring good cell distribution across such matrixes is a challenge. In preformed matrixes, cells need to be coaxed to distribute into the matrix interior by physical or biochemical means. Cell penetration is often limited, leading to excessive cell accumulation on matrix surfaces.[40] On the other hand, using a hydrogel system where cells can be incorporated during the gelation process, more homogeneous cell distribution throughout the matrix architecture can be achieved as we have shown in this study.

Cell number quantification in 3D cell cultures is a challenge.[31] Conventional 2D cell counting techniques are not always applicable in 3D. Assays based on cell metabolic activity or enzyme release have their drawbacks when applied to 3D cultures due to difficulties in ensuring homogeneous distribution of assay reagents to every cell, or effective harvesting of biomolecules from every cell, without altering cell physiology. Therefore, in 3D systems such as hydrogels, cell numbers are best measured by quantifying total dsDNA content within the cultures.[31] However, the accuracy of such fluorescent-based assays is further challenged by the autofluorescent nature of many protein-based 3D culture systems using collagen, elastin, and keratin.[41] In our case, both 1 mg/mL collagen and 25 mg/mL keratin hydrogel samples gave high background fluorescence (data not shown). Thus, we improvised by introducing a further phenol extraction step to remove the proteins after complete enzymatic digestion. Phenol extraction is a well-established technique in molecular biology that is used to extract nucleic acids from tissue samples, which are in fact natural cell-loaded protein-based scaffolds. Combining enzymatic digestion and phenol DNA extraction not only enhanced the accuracy of DNA quantification, but also provided a feasible strategy for future gene and protein expression studies.

Our results provide an early assessment of the cytocompatibility of keratin hydrogels as compared to collagen hydrogels. On the basis of our experimental conditions, the two hydrogels are comparable in terms of their ability to support L929 proliferation (Figures 3–5). It was also interesting that the keratin hydrogels contracted less as compared to the collagen hydrogels. However, we note that this difference in contractability could be due to the difference in protein content in the

DOI: 10.1021/acsami.5b00854
ACS Appl. Mater. Interfaces 2015, 7, 5187–5198

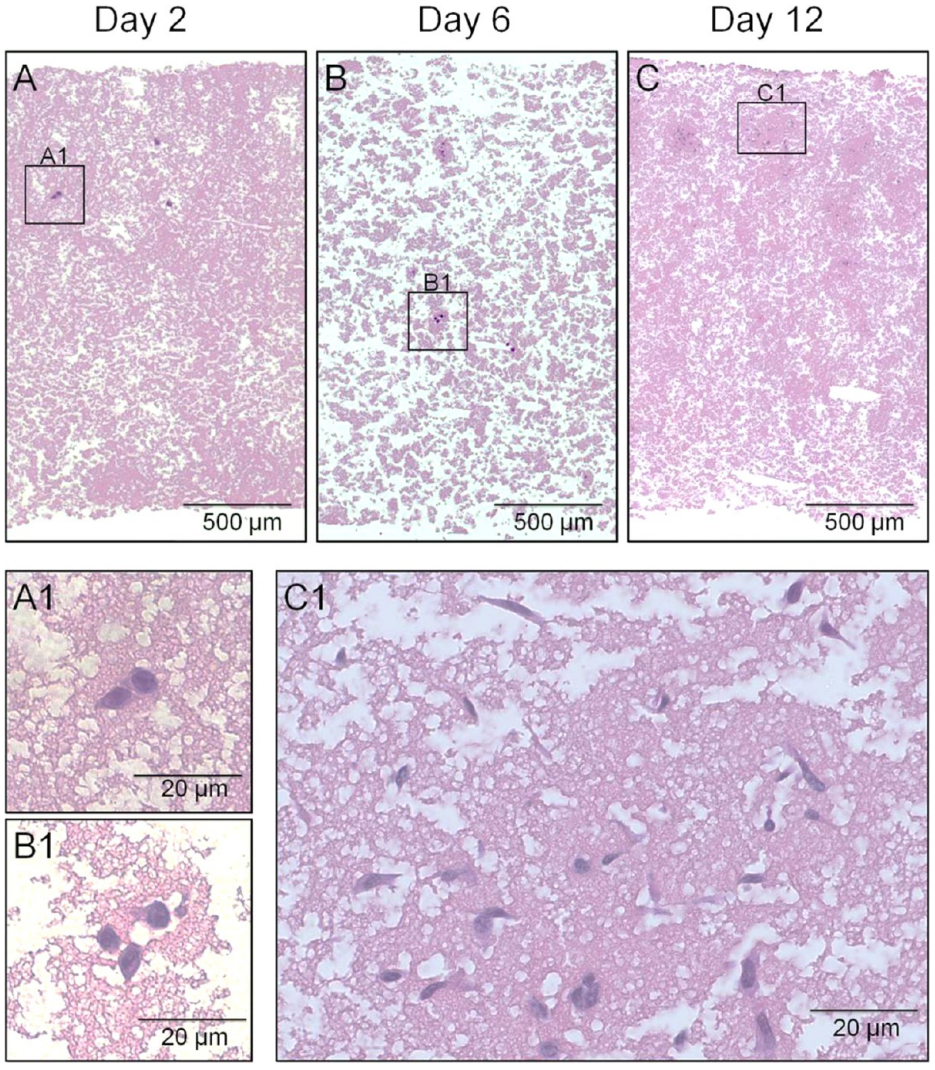

Figure 6. Histological analysis of cell-loaded keratin hydrogels. H&E stained cross sections at (A) days 2 and (B) 6 confirmed the random distribution of cells across the entire depth of the hydrogels. (C) At day 12, more cells were observed near the periphery of the samples. A1, B1, and C1 are the magnified views of the rectangular regions marked in panels A, B, and C, respectively.

keratin hydrogels (25 mg/mL) as compared to the collagen hydrogels (1 mg/mL), which had resulted in the keratin hydrogels being stiffer than the collagen hydrogels (data not shown). Nonetheless, others have reported that collagen-based hydrogels at high concentrations and stiffnesses could still be highly contracted or degraded in cell culture.[42−44]

Although we do not fully understand the mechanism, graft contraction could also be influenced by degradability of the hydrogels by proteases such as matrix metalloproteinases (MMPs) that are secreted by fibroblasts.[45] While it is well-established that collagens can be degraded by MMPs, it is not understood how keratins respond to them. Both our in vitro proteinase K digestion and in vivo animal study data suggest slow degradation of the keratin hydrogels. In addition, the keratin-specific enzyme, keratinase, is not naturally produced in the human body, suggesting that enzymatic digestion of keratin in the body could be less efficient.

Furthermore, graft contraction has been attributed to the differentiation of fibroblasts into contractile myofibroblasts.[40,46] The microenvironment and biochemical cues provided by the keratin hydrogels may play a role in regulating this differentiation and thus limiting contraction. In the context of wound healing, it is known that excessive graft contractions can lead to scar formation in vivo, which can lead to loss of tissue function, restriction of motion, and physical disfigurement.[47] It is therefore worthwhile to further investigate the potential and mechanism of the role of keratin hydrogels in preventing contraction, and if this is a viable approach to reduce scar formation.

5. CONCLUSIONS

In this study, we developed and optimized the procedure of producing human hair keratin-based hydrogels. We described the observed keratin flocculation process and identified three key factors (concentration, pH, temperature) that can be controlled to facilitate keratin gelation and living cell encapsulation. SEM images revealed a highly interconnected porous microarchitecture within the hydrogels. Oscillatory rheology measurements showed that keratin hydrogels could achieve stiffnesses similar to brain tissue. In vitro L929 culture studies demonstrated that cell viability was preserved during encapsulation and maintained across a 16 day culture period. However, cells tended to distribute toward the peripheral regions of the hydrogels due to diffusion limits. A method for dsDNA quantification in protein-based 3D cell cultures was developed to measure cell

DOI: 10.1021/acsami.5b00854
ACS Appl. Mater. Interfaces 2015, 7, 5187−5198

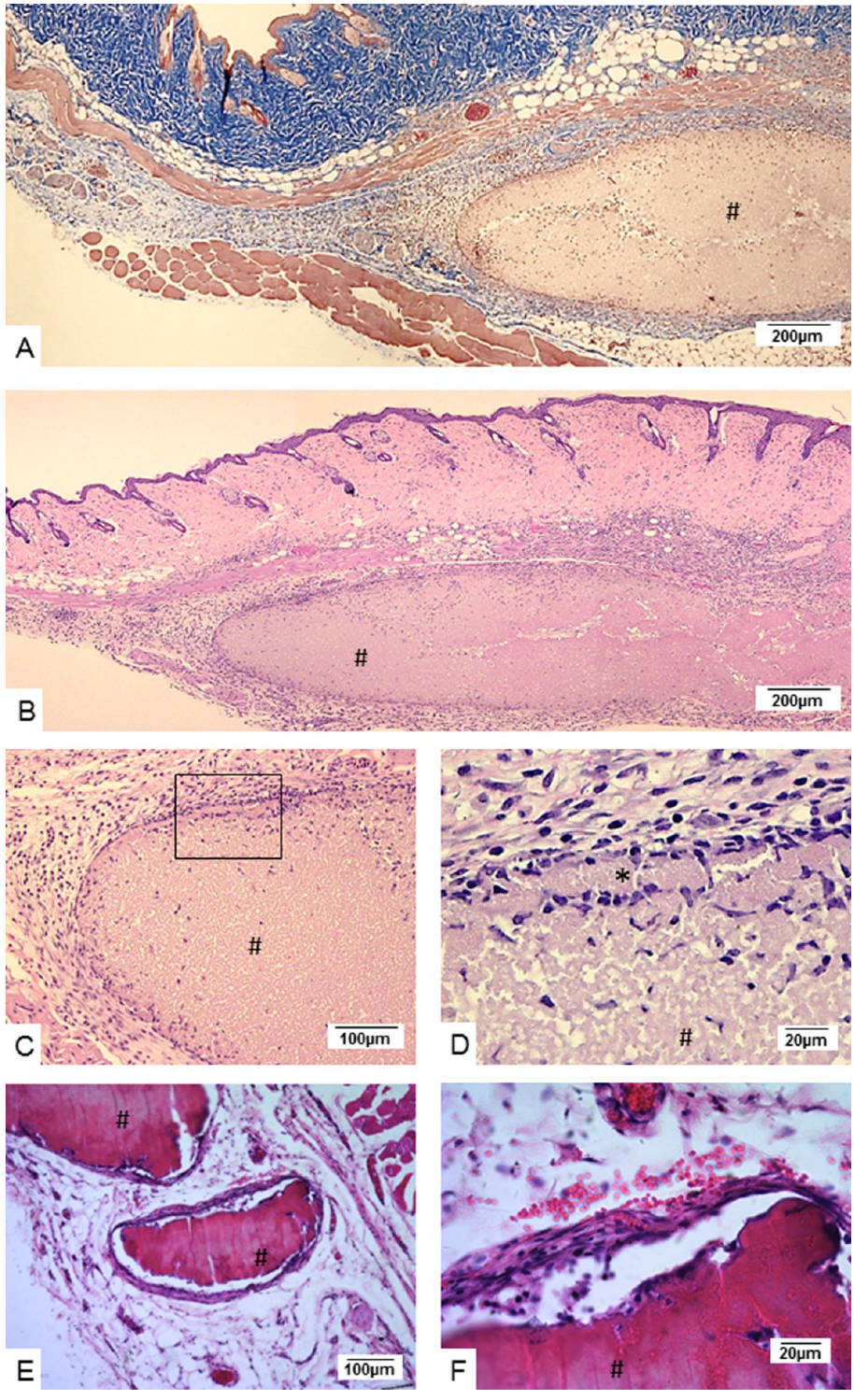

Figure 7. Subcutaneous implantation of keratin hydrogels into rodents. (A) Masson's Trichrome and (B–D) H&E stained keratin hydrogel sections at day 7 postimplantation in wild-type C57Bl/6 mice show intact implants (#), significant cell infiltration into the hydrogels, and mild fibrotic encapsulation. (B) Significant cell infiltration could be seen. (C) Magnified view of rectangular region marked out in panel (D) showing some tissue remodeling at the hydrogel-host tissue interface (*). (E and F) H&E stained sections after 90 days in Sprague–Dawley rats show fragmented implants and fibrotic encapsulation.

proliferation in the keratin hydrogels. Results suggest that keratin hydrogels were comparable to collagen hydrogels in terms of promoting L929 proliferation. The keratin hydrogels were also more capable of resisting contraction as compared to collagen hydrogels. Furthermore, the keratin hydrogels did not evoke acute host tissue response in vivo. The hydrogels were also slow degrading in vivo, retaining about 30% of their initial volume after 3 months. In conclusion, we demonstrate that human hair keratin hydrogels have tunable physical and mechanical properties, are cell compliant, do not evoke acute host tissue response, and therefore have potential to be used as an alternative 3D cell culture system.

DOI: 10.1021/acsami.5b00854
ACS Appl. Mater. Interfaces 2015, 7, 5187–5198

AUTHOR INFORMATION

Corresponding Authors

*Tel.: +86-21-34291002. Fax: +86-21-34292305. E-mail: mr.zhiyong@gmail.com.

*Tel.: +65-6513 8294. Fax: +65-6790-9081. E-mail: kwng@ntu.edu.sg.

Author Contributions

○S.W. and Z.W. contributed equally.

Notes

The authors declare no competing financial interest.

ACKNOWLEDGMENTS

We would like to acknowledge the funding support from the Ministry of Education, Singapore (RG42/13), to K.W.N. and the following funding support to Z.Z.: the National Natural Science Foundation of China (no. 81101353, no. 81371964), the Program for Professor of Special Appointment (Eastern Scholar) at Shanghai Institutions of Higher Learning (no. 1220000187), and the National Young Thousand-Talent Scheme and the Shanghai Rising-Star Program (13QA1402400).

REFERENCES

(1) Abbott, A. Cell Culture: Biology's New Dimension. *Nature* **2003**, *424*, 870−872.

(2) Pampaloni, F.; Reynaud, E. G.; Stelzer, E. H. K. The Third Dimension Bridges the Gap between Cell Culture and Live Tissue. *Nat. Rev. Mol. Cell Biol.* **2007**, *8*, 839−845.

(3) Santos, E.; Hernandez, R. M.; Pedraz, J. L.; Orive, G. Novel Advances in the Design of Three-Dimensional Bio-Scaffolds to Control Cell Fate: Translation from 2d to 3d. *Trends Biotechnol.* **2012**, *30*, 331−341.

(4) Leong, D. T.; Ng, K. W. Probing the Relevance of 3d Cancer Models in Nanomedicine Research. *Adv. Drug Delivery Rev.* **2014**, *79−80*, 95−106.

(5) Chien, K. B.; Aguado, B. A.; Bryce, P. J.; Shah, R. N. In Vivo Acute and Humoral Response to Three-Dimensional Porous Soy Protein Scaffolds. *Acta Biomater.* **2013**, *9*, 8983−8990.

(6) Wang, Y.; Rudym, D. D.; Walsh, A.; Abrahamsen, L.; Kim, H. J.; Kim, H. S.; Kirker-Head, C.; Kaplan, D. L. In Vivo Degradation of Three-Dimensional Silk Fibroin Scaffolds. *Biomaterials* **2008**, *29*, 3415−3428.

(7) Fields, G. B.; Lauer, J. L.; Dori, Y.; Forns, P.; Yu, Y. C.; Tirrell, M. Proteinlike Molecular Architecture: Biomaterial Applications for Inducing Cellular Receptor Binding and Signal Transduction. *Biopolymers* **1998**, *47*, 143−151.

(8) Altman, G. H.; Diaz, F.; Jakuba, C.; Calabro, T.; Horan, R. L.; Chen, J. S.; Lu, H.; Richmond, J.; Kaplan, D. L. Silk-Based Biomaterials. *Biomaterials* **2003**, *24*, 401−416.

(9) Lee, C. H.; Singla, A.; Lee, Y. Biomedical Applications of Collagen. *Int. J. Pharm.* **2001**, *221*, 1−22.

(10) Mulder, K. C. L.; Viana, A. a. B.; Xavier, M.; Parachin, N. S. Critical Aspects to Be Considered Prior to Large-Scale Production of Peptides. *Curr. Protein Pept. Sci.* **2013**, *14*, 556−567.

(11) Huang, C. J.; Lin, H.; Yang, X. M. Industrial Production of Recombinant Therapeutics in Escherichia Coli and Its Recent Advancements. *J. Ind. Microbiol. Biotechnol.* **2012**, *39*, 383−399.

(12) Lynn, A. K.; Yannas, I. V.; Bonfield, W. Antigenicity and Immunogenicity of Collagen. *J. Biomed. Mater. Res., Part B* **2004**, *71B*, 343−354.

(13) Rouse, J. G.; Van Dyke, M. E. A Review of Keratin-Based Biomaterials for Biomedical Applications. *Materials* **2010**, *3*, 999−1014.

(14) Wang, S.; Taraballi, F.; Tan, L.; Ng, K. Human Keratin Hydrogels Support Fibroblast Attachment and Proliferation in Vitro. *Cell Tissue Res.* **2012**, *347*, 795−802.

(15) Reichl, S. Films Based on Human Hair Keratin as Substrates for Cell Culture and Tissue Engineering. *Biomaterials* **2009**, *30*, 6854−6866.

(16) Verma, V.; Verma, P.; Ray, P.; Ray, A. R. Preparation of Scaffolds from Human Hair Proteins for Tissue-Engineering Applications. *Biomed. Mater. (Bristol, U. K.)* **2008**, *3*, 025007.

(17) Taraballi, F.; Wang, S.; Li, J.; Lee, F. Y.; Venkatraman, S. S.; Birch, W. R.; Teoh, S. H.; Boey, F. Y.; Ng, K. W. Understanding the Nano-Topography Changes and Cellular Influences Resulting from the Surface Adsorption of Human Hair Keratins. *Adv. Healthcare Mater.* **2012**, *1*, 513−519.

(18) Reichl, S.; Borrelli, M.; Geerling, G. Keratin Films for Ocular Surface Reconstruction. *Biomaterials* **2011**, *32*, 3375−3386.

(19) Katoh, K.; Tanabe, T.; Yamauchi, K. Novel Approach to Fabricate Keratin Sponge Scaffolds with Controlled Pore Size and Porosity. *Biomaterials* **2004**, *25*, 4255−4262.

(20) Tachibana, A.; Furuta, Y.; Takeshima, H.; Tanabe, T.; Yamauchi, K. Fabrication of Wool Keratin Sponge Scaffolds for Long-Term Cell Cultivation. *J. Biotechnol.* **2002**, *93*, 165−170.

(21) Kurimoto, A.; Tanabe, T.; Tachibana, A.; Yamauchi, K. Keratin Sponge: Immobilization of Lysozyme. *J. Biosci. Bioeng.* **2003**, *96*, 307−309.

(22) Cilurzo, F.; Selmin, F.; Aluigi, A.; Bellosta, S. Regenerated Keratin Proteins as Potential Biomaterial for Drug Delivery. *Polym. Adv. Technol.* **2013**, *24*, 1025−1028.

(23) Hirao, Y.; Ohkawa, K.; Yamamoto, H.; Fujii, T. A Novel Human Hair Protein Fiber Prepared by Watery Hybridization Spinning. *Macromol. Mater. Eng.* **2005**, *290*, 165−171.

(24) Sow, W. T.; Lui, Y. S.; Ng, K. W. Electrospun Human Keratin Matrices as Templates for Tissue Regeneration. *Nanomedicine (London, U. K.)* **2013**, *8*, 531−541.

(25) Bhardwaj, N.; Sow, W. T.; Devi, D.; Ng, K. W.; Mandal, B. B.; Cho, N.-J. Silk Fibroin-Keratin Based 3d Scaffolds as a Dermal Substitute for Skin Tissue Engineering. *Integr. Biol.* **2015**, *7*, 53−63.

(26) Silva, R.; Fabry, B.; Boccaccini, A. R. Fibrous Protein-Based Hydrogels for Cell Encapsulation. *Biomaterials* **2014**, *35*, 6727−6738.

(27) Aboushwareb, T.; Eberli, D.; Ward, C.; Broda, C.; Holcomb, J.; Atala, A.; Van Dyke, M. A Keratin Biomaterial Gel Hemostat Derived from Human Hair: Evaluation in a Rabbit Model of Lethal Liver Injury. *J. Biomed. Mater. Res., Part B* **2009**, *90B*, 45−54.

(28) Hill, P. S.; Apel, P. J.; Barnwell, J.; Smith, T.; Koman, L. A.; Atala, A.; Van Dyke, M. Repair of Peripheral Nerve Defects in Rabbits Using Keratin Hydrogel Scaffolds. *Tissue Eng., Part A* **2011**, *17*, 1499−1505.

(29) Burnett, L. R.; Richter, J. G.; Rahmany, M. B.; Soler, R.; Steen, J. A.; Orlando, G.; Abouswareb, T.; Van Dyke, M. E. Novel Keratin (Kerastat (Tm)) and Polyurethane (Nanosan (R)-Sorb) Biomaterials Are Hemostatic in a Porcine Lethal Extremity Hemorrhage Model. *J. Biomater. Appl.* **2014**, *28*, 869−879.

(30) Wang, S.; Taraballi, F.; Tan, L. P.; Ng, K. W. Human Keratin Hydrogels Support Fibroblast Attachment and Proliferation in Vitro. *Cell Tissue Res.* **2012**, *347*, 795−802.

(31) Ng, K. W.; Leong, D. T. W.; Hutmacher, D. W. The Challenge to Measure Cell Proliferation in Two and Three Dimensions. *Tissue Eng.* **2005**, *11*, 182−191.

(32) Ng, K. W.; Hutmacher, D. W. Reduced Contraction of Skin Equivalent Engineered Using Cell Sheets Cultured in 3d Matrices. *Biomaterials* **2006**, *27*, 4591−4598.

(33) Ng, K. W.; Tham, W.; Lim, T. C.; Werner Hutmacher, D. Assimilating Cell Sheets and Hybrid Scaffolds for Dermal Tissue Engineering. *J. Biomed. Mater. Res., Part A* **2005**, *75*, 425−438.

(34) Rashid, B.; Destrade, M.; Gilchrist, M. D. Mechanical Characterization of Brain Tissue in Simple Shear at Dynamic Strain Rates. *J. Mech. Behav. Biomed. Mater.* **2013**, *28*, 71−85.

(35) Daintith, J. *A Dictionary of Chemistry*, 6th ed.; Oxford University Press: New York, 2008.

(36) Slomkowski, S.; Aleman, J. V.; Gilbert, R. G.; Hess, M.; Horie, K.; Jones, R. G.; Kubisa, P.; Meisel, I.; Mormann, W.; Penczek, S.; Stepto, R. F. T. Terminology of Polymers and Polymerization Processes in

DOI: 10.1021/acsami.5b00854
ACS Appl. Mater. Interfaces 2015, 7, 5187−5198

Dispersed Systems (Iupac Recommendations 2011). *Pure Appl. Chem.* **2011**, *83*, 2229−2259.
(37) Banerjee, S.; Bhattacharya, S. Food Gels: Gelling Process and New Applications. *Crit. Rev. Food Sci. Nutr.* **2011**, *52*, 334−346.
(38) Totosaus, A.; Montejano, J. G.; Salazar, J. A.; Guerrero, I. A Review of Physical and Chemical Protein-Gel Induction. *Int. J. Food Sci. Technol.* **2002**, *37*, 589−601.
(39) Lee, J.; Cuddihy, M. J.; Kotov, N. A. Three-Dimensional Cell Culture Matrices: State of the Art. *Tissue Eng., Part B* **2008**, *14*, 61−86.
(40) Ng, K. W.; Khor, H. L.; Hutmacher, D. W. In Vitro Characterization of Natural and Synthetic Dermal Matrices Cultured with Human Dermal Fibroblasts. *Biomaterials* **2004**, *25*, 2807−2818.
(41) Billinton, N.; Knight, A. W. Seeing the Wood through the Trees: A Review of Techniques for Distinguishing Green Fluorescent Protein from Endogenous Autofluorescence. *Anal. Biochem.* **2001**, *291*, 175−197.
(42) Berendsen, A. D.; Bronckers, A. L. J. J.; Smit, T. H.; Walboomers, X. F.; Everts, V. Collagen Type V Enhances Matrix Contraction by Human Periodontal Ligament Fibroblasts Seeded in Three-Dimensional Collagen Gels. *Matrix Biol.* **2006**, *25*, 515−522.
(43) Zhu, Y. K.; Umino, T.; Liu, X. D.; Wang, H. J.; Romberger, D. J.; Spurzem, J. R.; Rennard, S. I. Contraction of Fibroblast-Containing Collagen Gels: Initial Collagen Concentration Regulates the Degree of Contraction and Cell Survival. *In Vitro Cell. Dev. Biol.: Anim.* **2001**, *37*, 10−16.
(44) Abreu, E. L.; Palmer, M. P.; Murray, M. M. Collagen Density Significantly Affects the Functional Properties of an Engineered Provisional Scaffold. *J. Biomed. Mater. Res., Part A* **2010**, *93A*, 150−157.
(45) Abraham, L. C.; Dice, J. F.; Lee, K.; Kaplan, D. L. Phagocytosis and Remodeling of Collagen Matrices. *Exp. Cell Res.* **2007**, *313*, 1045−1055.
(46) Spector, M. Novel Cell-Scaffold Interactions Encountered in Tissue Engineering: Contractile Behavior of Musculoskeletal Connective Tissue Cells. *Tissue Eng.* **2002**, *8*, 351−357.
(47) Corin, K. A.; Gibson, L. J. Cell Contraction Forces in Scaffolds with Varying Pore Size and Cell Density. *Biomaterials* **2010**, *31*, 4835−4845.

DOI: 10.1021/acsami.5b00854
ACS Appl. Mater. Interfaces 2015, 7, 5187−5198